

# Monte-Carlo simulations of polymer crystallization in dilute solution

C.-M. Chen<sup>a)</sup> and Paul G. Higgs

*School of Biological Sciences, University of Manchester, Manchester M13 9PT, United Kingdom*

(Received 7 July 1997; accepted 8 December 1997)

Polymer crystallization in dilute solution is studied by three-dimensional Monte-Carlo simulations using the bond fluctuation model. We study monodisperse chains of moderate length, intended to model recent experiments on monodisperse alkanes with length of a few hundred carbon atoms, and we also investigate chain folding of very long polymers. For monodisperse flexible chains we observe both extended-chain and once-folded-chain crystals. The simulations illustrate the range of defects and irregularities which we expect to find in polymer crystals. The roughness of the top and bottom surfaces of the lamellae is measured. Chain ends can be seen as cilia emerging from the surfaces. Folds are found to occur with approximately equal frequency on top and bottom surfaces. Although most chain folds are aligned perpendicular to the growth direction, a significant number of chains folding parallel to the growth direction are found as defects. The simulation includes a chain stiffness parameter which has an important effect on chain folding kinetics. When chains are semi-flexible the crystals formed are extremely irregular with many defects including holes and blocks of extended chains within the folded chain lamellae. For very long chains we show that the lamellar thickness is determined by the folding kinetics. The thickness diverges as the temperature approaches the infinite chain melting point  $T_\infty$ . For  $T \rightarrow T_\infty$ , the thickness is close to the theoretical minimum thickness, which indicates the dominant importance of the entropic barrier in crystallization. © 1998 American Institute of Physics. [S0021-9606(98)52510-X]

## I. INTRODUCTION

The study of polymer crystallization has received considerable attention since the discovery of crystallization of thin lamellar polymer crystals in solution in 1957. For a recent review see Ref. 1. In general, polymers can form two-dimensional lamellar crystals in both melts and solution. The crystal thickness decreases continuously with supercooling for polydisperse polymer chains, and is mainly determined by folding kinetics rather than by energetics: although thick crystals are thermodynamically more stable than thin crystals, thin crystals can grow faster than thick crystals at large supercoolings.

There are many attempts to explain the physical origin of polymer crystallization. The secondary nucleation theory of crystallization<sup>2</sup> is a coarse-grained model which correctly predicts the growth rate of crystallization for polydisperse polymers. The nucleation barrier has now been recognized to be entropic.<sup>3</sup> Various modifications of the nucleation theory have been applied to study morphology of the crystal,<sup>4-6</sup> fractionation,<sup>7</sup> and layer thickening.<sup>8</sup> An alternative fine-grained model takes a rather different approach involving rough growth surfaces and molecular pinning.<sup>9-11</sup> Crystal thickness and growth rate calculated from this model are in agreement with results of the nucleation theory. The above models provide simplified views of polymer crystallization. A more realistic picture of polymer crystallization is desired to include both chain connectivity and entropic barrier.

The discussion above applies to polymer crystallization

in polydisperse systems. However, recent experiments on monodisperse alkane chains<sup>12</sup> show anomalous growth rate of crystallization<sup>13,14</sup> and a marked preference for "integer folding."<sup>15</sup> Crystallization of monodisperse alkanes has recently attracted considerable interest both experimentally and theoretically. For temperatures lower than  $T_1$  (the crystallization temperature of extended chain crystals), the growth rate initially increases with supercooling, passes through a maximum, and falls to a minimum at a temperature  $T_2$  (the crystallization temperature of folded chain crystals). Below  $T_2$ , the growth rate increases sharply with supercooling. Real-time small angle x-ray scattering experiments show that extended chain crystals form at temperatures between  $T_1$  and  $T_2$ , and once-folded chain crystals form at temperatures below  $T_2$ .<sup>13</sup> This anomalous temperature dependence of growth rate is interpreted by the so called "self-poisoning" effect, which is due to wrongly folded chains on the crystal surfaces preventing the adsorption of further correctly positioned chains. Sadler and Gilmer modified their row model by including a preferred thickness which seems to give correct trends of the growth rate in monodisperse systems.<sup>16</sup> Although this model might not provide a true representation of polymer crystallization, it does mimic the "self-poisoning effect" in crystal growth.

Previously we presented a model<sup>17</sup> to describe the self-poisoning effect in monodisperse alkane crystallization and the minimum in the growth curve. The one-dimensional version of this model is simple enough to solve the growth rate analytically. The two-dimensional version, representing the growth of one single lamella, was studied by Monte-Carlo simulations. In this paper, we study the kinetics of chain folding during polymer crystallization in dilute solution by

<sup>a)</sup>Present address: Department of Physics, National Taiwan Normal University, Taipei 11718, Taiwan, Republic of China.

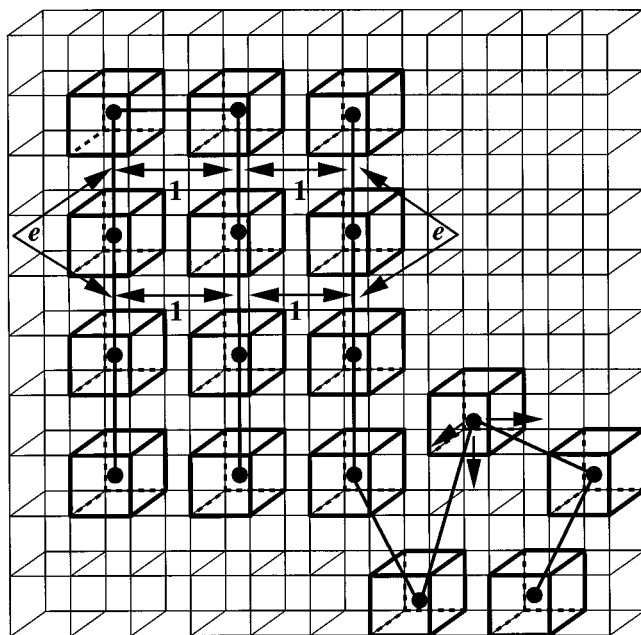


FIG. 1. 2 chains of 8 monomers are shown. All monomers are shown in one plane for convenience although the simulations are done in 3D. Attractive interactions of strength 1 occur whenever there are two parallel  $P(2,0,0)$  nonsuccessive bonds on neighboring lattice sites. The bond may be on the same chain or different chains. An attractive energy  $e$  is also added whenever two successive bonds on the same chain are parallel and are both  $P(2,0,0)$ .

three-dimensional Monte-Carlo simulations using the bond-fluctuation model. The method of Monte-Carlo simulations for polymer crystallization is described in Sec. II. In Sec. III, we discuss the results from Monte-Carlo simulations for monodisperse flexible polymer chains at different temperatures. The effect of chain stiffness of polymers is discussed in Sec. IV. In Sec. V, we study the crystallization of extremely long polymer chains in dilute solution. Section VI contains the discussion and conclusions of this paper.

## II. ALGORITHM OF MONTE-CARLO SIMULATION

The bond fluctuation model is an efficient method of simulating the dynamics of large numbers of polymer chains. It was originally introduced by Carmesin and Kremer<sup>18</sup> for studying dynamics of polymer chains in various spatial dimensions. Since then it has been used for investigation of the crossover between Rouse and reptation dynamics,<sup>19</sup> for studying interdiffusion of polymer blends,<sup>20</sup> and the dynamics of polymer melts near glass transition.<sup>21</sup>

Each monomer in the model occupies a  $2 \times 2 \times 2$  cube of sites on a cubic lattice (see Fig. 1). The set of allowed bond vectors is

$$\mathbf{B} = P(2,0,0) \cup P(2,1,0) \cup P(2,1,1) \cup P(3,0,0) \cup P(3,1,0), \quad (1)$$

where  $P(a,b,c)$  stands for the set of all permutations and sign combinations of  $\pm a, \pm b, \pm c$ . The number of configurations per bond is  $z = 108$ . The length of one bond can take any one of the 5 values  $2, \sqrt{5}, \sqrt{6}, 3, \sqrt{10}$  (in units of lattice spacing). Chains satisfy the excluded volume constraint: no

lattice site may be occupied by more than one monomer. Each attempted move is to move one monomer by one lattice site in one of the 6 lattice directions. The move is rejected if the new position breaks the excluded volume constraint, or if the new bond vectors between the monomer which was moved and its neighbors are not contained in the set  $\mathbf{B}$ . The set  $\mathbf{B}$  is chosen to satisfy the constraints of both excluded volume between monomers and topological entanglement between chains (i.e., two chains cannot pass through each other). If any other bond vectors were added to this set, the chains would become ‘‘phantom’’ chains.

In order to model crystallization we have added attractive interactions between chains which are different from those used in the previous studies.<sup>20,22</sup> Polymer crystals contain arrays of parallel stems held together by short range attractive forces. This is modeled by an attractive interaction of energy  $-1$  unit whenever there are two parallel  $P(2,0,0)$  bonds (non-successive) on neighboring sites. In addition there is an energy of  $-e$  whenever there are two successive parallel  $P(2,0,0)$  bonds on the same chain (see Fig. 1). This additional energy is to model the energy difference between *gauche* and *trans* bonds of polymer chains (or equivalently the kink energy).

Simulations are carried out at a constant temperature  $T$  using the Metropolis algorithm. If any attempted move of monomers satisfies the excluded volume constraint and the new bond vectors are still in the allowed set, then the move is accepted with probability

$$w = \min[1, \exp(-\Delta E/T)]. \quad (2)$$

The two parameters in the model are the temperature  $T$  and the stiffness parameter  $e$ . If  $T/e \gg 1$  and  $T$  is not much less than 1, the chain behaves like a self avoiding walk. If  $T/e \ll 1$  the chain will be rod-like. In order to determine appropriate parameter ranges for the simulation, we measured the angular correlations between nearest neighboring bonds ( $f_1$ ) and next nearest neighboring bonds ( $f_2$ ) as a function of  $T/e$  (as shown in Fig. 2), where  $f_1 \equiv \langle \mathbf{u}_i \cdot \mathbf{u}_{i+1} \rangle_{\text{en}}$ ,  $f_2 \equiv \langle \mathbf{u}_i \cdot \mathbf{u}_{i+2} \rangle_{\text{en}}$ , and  $\mathbf{u}_i$  is the unit vector of the  $i$ -th bond. The angular bracket  $\langle \rangle_{\text{en}}$  indicates an ensemble average over all possible configurations weighted by their Boltzmann probabilities. Figure 2 shows that for  $T/e > 0.3$  there is almost no change in these correlations. Both  $f_1$  and  $f_2$  have small positive values at large  $T/e$  which are due to excluded volume constraints only but not the stiffness energy term. For  $T/e < 0.3$  the chain is significantly stiffened by the stiffness energy term. In all simulations presented in this paper  $0.5 < T/e < 0.7$  so that the chains in solution behave like flexible self-avoiding walks.

The parameter  $e$  has another role in this model which is actually more important than controlling the stiffness of the chains in solution, and it is for this reason that we include it in the simulation. The value of  $e$  affects polymer crystallization in the following two ways: (1) it lowers the free energy of the crystals, and therefore we expect that the crystallization temperature of polymeric crystals increases with  $e$ ; (2) it penalizes folding of polymer chains, and we expect a different folding kinetics at large values of  $e$ . The second point is particularly important for temperatures below  $T_2$  since the

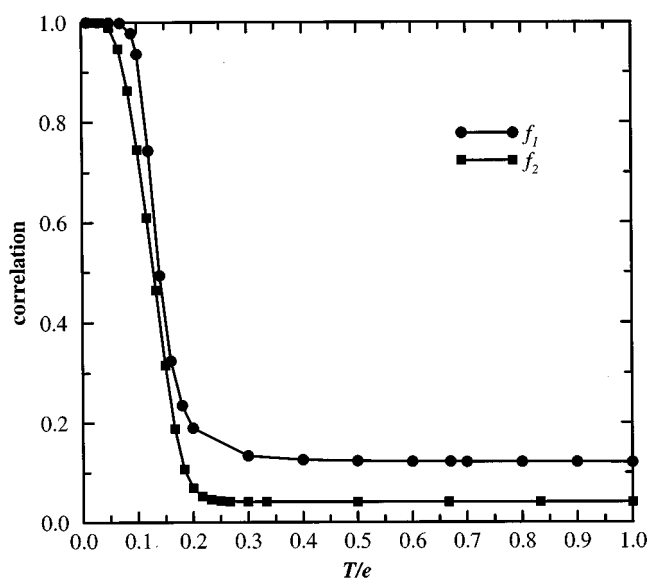


FIG. 2. Angular correlations between nearest neighboring bonds ( $f_1$ ) and next nearest neighboring bonds ( $f_2$ ) as a function of  $T/e$ . For  $T/e > 0.3$ , both correlations are not affected by the stiffness parameter  $e$ . For  $T/e < 0.3$ , the persistence length of polymer chains is longer than the bond length.

resulting crystal is determined by the competition between folding kinetics and chain stiffness.

### III. CRYSTALLIZATION OF MONODISPERSE FLEXIBLE POLYMER CHAINS

As discussed in the Introduction, for monodisperse alkane chains “integer folding” of polymer crystallization is observed in various experiments. In this section, we simulate the folding kinetics of polymer crystallization for polymer chains with chain stiffness parameter  $e=0.6$  at temperatures between  $T_1$  and  $T_2$  and at temperatures below  $T_2$ .

Simulations were done in a box of  $40 \times 10 \times 32$  with the periodic boundary condition in both  $x$ - and  $z$ -axes, and the hard wall boundary condition in  $y$ -axis. Chains in the crystal are aligned in the  $z$  direction and crystal growth is in the  $y$  direction. In the box, 10 polymer chains with 8 effective monomers per chain were deposited randomly, and hence the concentration of polymer chains is  $\phi \approx 0.006$ . The initial nucleation will not be discussed in this paper, and we use two different seeds to study the growth of crystals after nucleation. The seed can be a layer of extended chains (seed thickness  $l_{\text{seed}} = 8$  monomers) or once-folded chains ( $l_{\text{seed}} = 4$  monomers) in the  $x-z$  plane. During the simulation, polymer chains are constantly adsorbed or released from the crystal surfaces (growing from the seed). The size of the box in  $y$ -direction increases according to the propagation of the growth front of the crystal so that the total volume of accessible space for polymer chains is roughly fixed. Additional polymer chains were added into the box as soon as the number of free polymer chains in solution is less than 10, so that the concentration of polymer chains is approximately constant.

In Fig. 3, we show the growth rate, attachment and detachment rate as a function of time during the crystallization

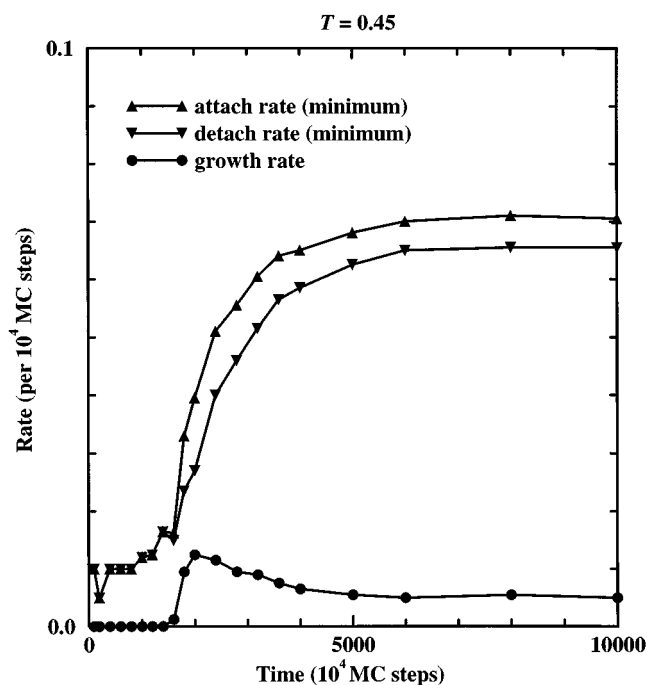


FIG. 3. Growth rate, attach rate, and detach rate of polymer chains with  $e=0.6$  during crystallization at  $T=0.45$ . The attach rate increases sharply after nucleating an additional layer at  $T \sim 10^5$  MC steps. The growth rate overshoots right after the nucleation due to the concentration fluctuation of polymer chains. The small attach rate indicates a complicated folding kinetics of polymer chains near the crystal surface.

of polymer chains with stiffness parameter  $e=0.6$  at  $T=0.45$ . The attachment and detachment rates are defined by the number of chains which have successfully attached to (or detached from) the crystal surface divided by total time since the beginning of the simulation. A monomer is counted as being part of the crystal if at least 3 of the sites which would be nearest neighbors in the crystal are occupied by monomers. A chain is counted as being attached to the crystal if more than half of its monomers are in the crystal. We count the number of attached (detached) polymer chains every  $2 \times 10^4$  Monte-Carlo (MC) steps (where one MC step represents an average of one attempted move per monomer), therefore the measured values are slight underestimates, due to the possibility of a chain attaching and detaching in the same time period. The growth rate is the difference between attachment and detachment rates. This is not affected by the possible cancellation of attaching and detaching of polymer chains. The initial growth rate is very small due to the difficulty of nucleating an additional layer on a flat surface. The attachment rate increases sharply after the nucleation of an additional layer due to the increased surface roughness. At long times, the average growth rate is about 0.005 chains per  $10^4$  MC steps. The growth rate is much slower than the chain attachment and detachment rates, indicating that there is a large amount of reorganization of chain configurations going on at the crystal surface, and that each chain moves on and off the surface several times before finding its final position. The chain attachment rate is itself very slow (only 0.07 per  $10^4$  MC steps), which emphasizes the very large number of

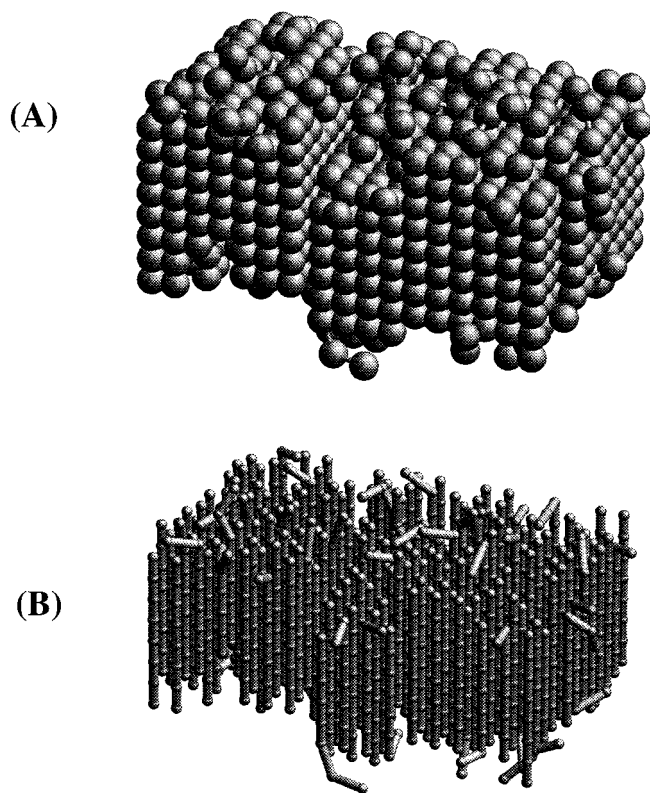


FIG. 4. Monte-Carlo simulation of an extended chain crystal of chains of length 8 effective monomers grown from an extended chain seed: (A) a "space filling" representation which shows surface clearly, and (B) an alternative representation of the same configuration, which shows the bond configurations. In the simulation,  $T=0.45$  and  $e=0.6$ . Both surface roughness and cilia of the crystal can be easily seen. The seed layer is at the rear of this view (not shown) and the growth direction ( $y$  axis) is toward the viewer.

individual monomer moves which are involved.

In the Appendix, we estimate that  $T_1 \approx 0.48$  and  $T_2 \approx 0.41$  for stiffness parameter  $e=0.6$  and concentration of polymer chains  $\phi=0.006$ . Figure 4 shows the surfaces (A) and bond configurations (B) of an extended chain crystal, forming at  $T=0.45$ . The simulation was performed with a seed of extended chains. No crystallization is seen if the seed has only half-length since a folded chain crystal is unstable at this temperature. For the crystal shown in Fig. 4, the surface roughness is about  $1.8 \pm 0.05$  (lattice spacing). Here we define the surface roughness as the standard deviation of the surface position of each stem, i.e.,  $\sigma = \sqrt{(\bar{z}^2 - \bar{z}^2)}$ , where  $\bar{z}$  is the average of surface position of each stem  $z_{i,j}$  ( $j$ -th stem on the  $i$ -th layer). A monomer is considered to be part of the crystal if more than three of its nearest neighboring sites are occupied by other monomers.  $z_{i,j}$  is calculated by considering only those monomers in the crystal but not those in cilia. There are no folded chains in this crystal. We expect that the surface roughness will become smaller at higher temperatures since rough extended chain crystals are less stable than solution. The layer thickness of the above extended chain crystal is 7.65 monomers which is close to the full chain length. In Fig. 5, we show the relative density (normalized to 1) of the extended chain crystal. The origin is chosen to be

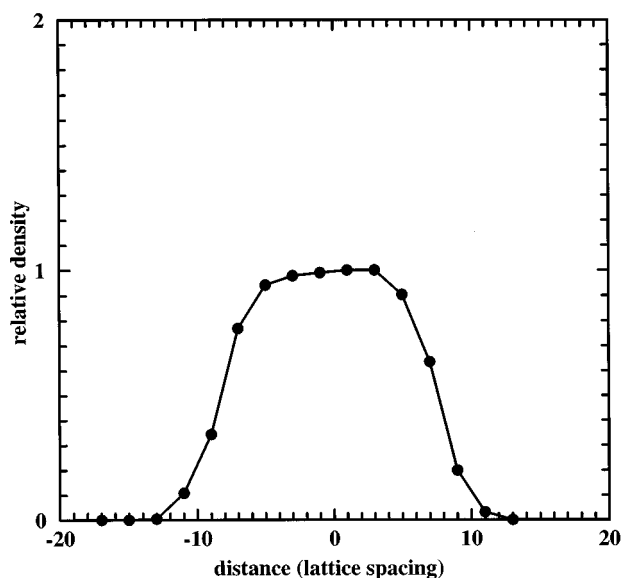


FIG. 5. Density profile of an extended chain crystal as a function of distance away from the center of the seed. The seed layer extends from  $-7$  to  $7$ .

the center of the seed. The density profile of the extended chain crystal decreases slowly to zero at the boundaries due to surface roughness and cilia.

Figure 6 shows the surfaces (A) and bond configurations (B) of a folded chain crystal, forming at  $T=0.4$ . The simulation was performed with a seed of fold chains and all folds on the bottom surface. However, we also consider the crystallization with a seed of extended chains at the same temperature, and the resulting crystal is shown in Fig. 7. This initial condition can be achieved by first quenching the system to a temperature between  $T_1$  and  $T_2$ , and then quenching it again to a temperature below  $T_2$ . For the resulting folded chain crystal shown in Fig. 6, the surface roughness is about  $0.47 \pm 0.07$  (lattice spacing). The number of folds parallel to the seed is 53 on the top surface and 48 on the bottom surface. The number of folds perpendicular to the seed is 11 on the top surface and 13 on the bottom surface. Although the symmetry between top and bottom surfaces is deliberately broken by the initial condition, the resulting crystal restores this symmetry immediately after 5 layers. Here we define the asymmetry of folding by  $a(l) = (n_{b\parallel} - n_{t\parallel}) / (n_{b\parallel} + n_{t\parallel})$ , where  $l$  is number of layers in the crystal, and  $n_{b\parallel}$  and  $n_{t\parallel}$  are the number of folds parallel to the seed on the bottom surface and the top surface respectively. As shown in Fig. 8, for the folded chain crystal growing from a seed of folded chains, the asymmetry drops to zero very quickly due to kinetics. For the folded chain crystal growing from a seed of extended chains, the asymmetry of folding is essentially zero but there are fluctuations due to finite size effects. In this example 19% of chains are folded forward, i.e., perpendicular to the seed, which is surprisingly high. These forward folds can occur if the neighboring stems of a half attached chain on the same layer are occupied by other chains. Therefore the number of folds perpendicular to the seed should increase with concentration. We suspect that the simulation gives a much larger fraction of forward folded chains than in

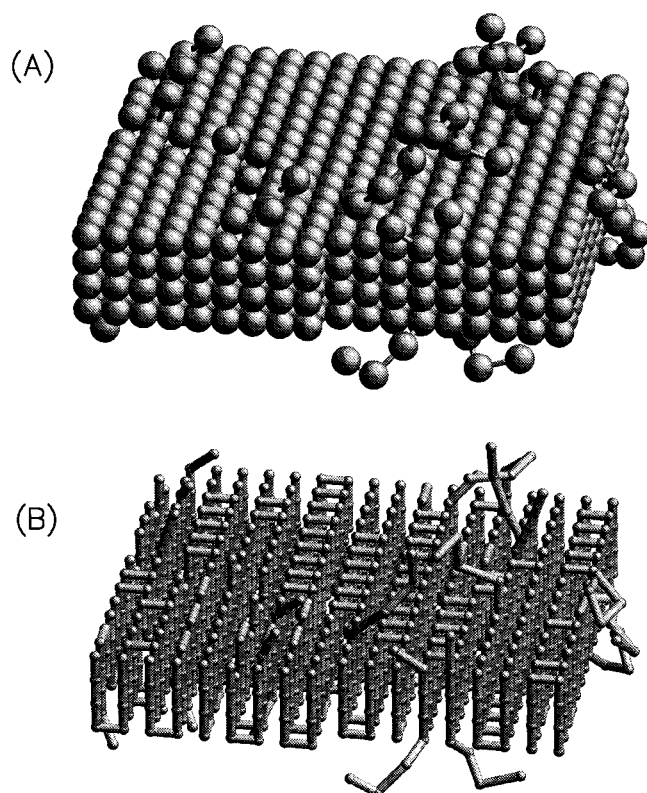


FIG. 6. Schematic representations of surfaces (A) and bond configurations (B) of a folded chain crystal obtained from the Monte-Carlo simulation with a seed of folded chains at  $T=0.4$ . The stiffness parameter of polymer chains is  $e=0.6$ . Both surface roughness and cilia of the crystal can be easily seen. Folds occur on both top and bottom surfaces. Defects can also be seen where the fold direction is parallel to the crystal growth direction.

real crystals, but it would nevertheless be interesting to try to measure this experimentally.

The layer thickness and relative density of folded chain crystals are shown in Figs. 9 and 10. In Fig. 9, the thickness of each layer is roughly 4 monomers for the folded chain crystal growing from a folded chain seed. For the folded chain crystal growing from an extended chain seed, the average layer thickness decreases from 8 monomers to 4 monomers. In Fig. 10, for the crystal growing from a folded chain seed, the density profile of the crystal has sharp boundaries at both top and bottom surfaces. The tails of the density profile are due to cilia. For the crystal growing from an extended chain seed, the boundaries are much less sharp. The density profile of the crystal is due to a mismatch between the left and right halves of the crystal by one monomer (2 lattice spacings) as shown in Fig. 7. Moreover, the density profile is not centered at the origin since the major half of the crystal is located above the center of the seed.

#### IV. EFFECTS OF CHAIN STIFFNESS PARAMETER ON CRYSTALLIZATION

In the previous example of folded chain crystallization  $e=0.6$  and  $T=0.4$ , so that  $T/e=0.67$ . This is in the region where the chains appear to be behaving as flexible self-avoiding walks in solution (see Fig. 2). Since it is possible

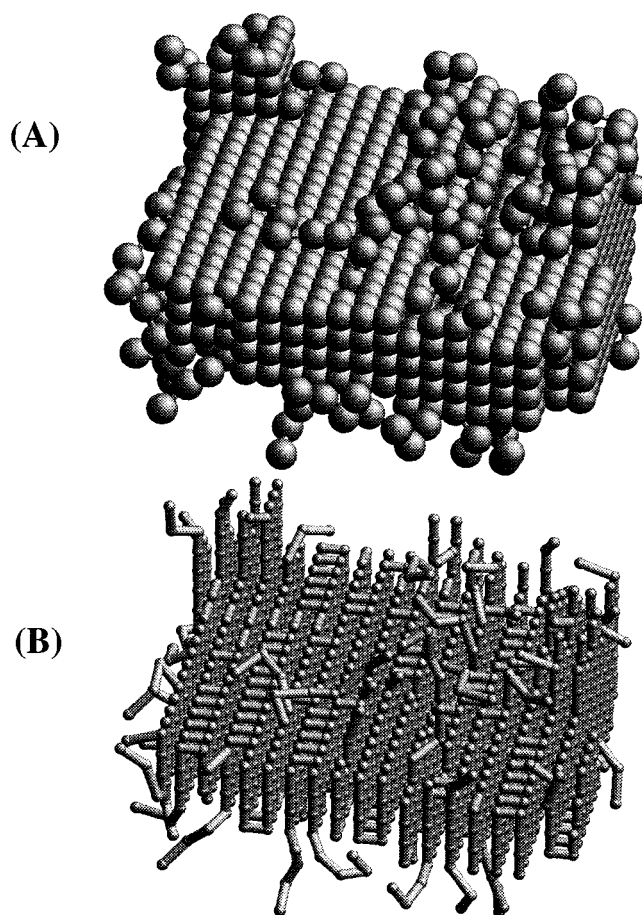


FIG. 7. Schematic representations of surfaces (A) and bond configurations (B) of a folded chain crystal obtained from the Monte-Carlo simulation with a seed of extended chains. Temperature and chain stiffness are as in Fig. 6. The chains have begun to fold already in the first layer and after a few layers a folded chain crystal similar to Fig. 6 is seen.

for folded chain crystals to form at this value of  $e$  it will also be possible for folded chain crystals to form with lower values of  $e$  and the same chain length, or for longer chain lengths at the same value of  $e$ . However we might expect chains with larger  $e$  to have difficulty in forming folded chain crystals.

Figure 11 shows the results of a simulation using a folded chain seed with  $e=0.8$ , and with  $T$  kept at 0.4 so that  $T/e$  is reduced to 0.5. The single chain is still flexible according to Fig. 2, and the angular correlation is hardly any different from the previous case. However there is a substantial difference in the crystal properties (cf. Figs. 11 and 6). There are now many defects in the crystal including some holes and some extended chains within the folded chain crystal. The average thickness increases from 4 at the seed to about 5 after 10 layers due to the presence of these extended chains. This temperature still lies below  $T_2$ , so that we should still expect folded chain crystals. If we begin with an extended chain seed (thickness 8) the mean crystal thickness decreases to about 6 after only a few layers.

Figure 12 shows the density of profiles in this case. When  $l_{\text{seed}}=4$  there is a similar pattern to Fig. 10 due to mismatch between two blocks of crystal at different heights.

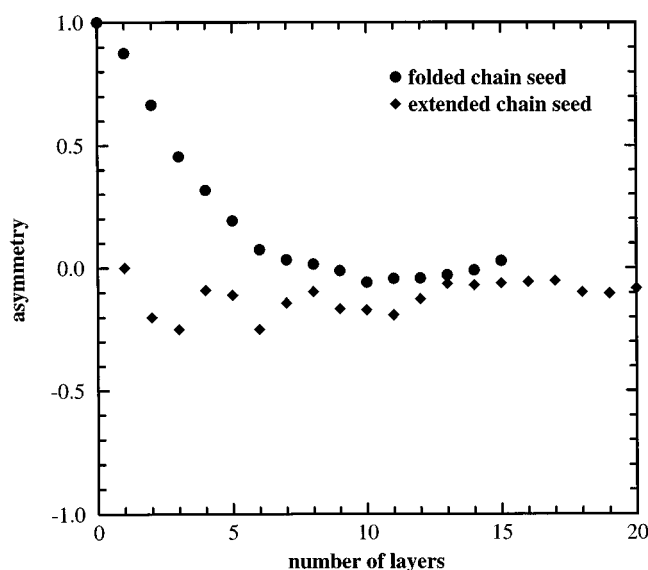


FIG. 8. Folding asymmetry of folded chain crystals growing from a symmetric seed and an asymmetric seed. In both cases, the folding asymmetry becomes smaller as the crystals grow.

When  $l_{\text{seed}}=8$  the profile is extremely broad. Both of these profiles represent extremely irregular crystals in comparison to those obtained with  $e=0.6$ . This indicates that the crystallization process in the simulation is extremely sensitive to the rates of the different types of Monte-Carlo moves which occur. Increasing  $e$  generally makes reorganization of chain configurations on the surface more difficult, and leads to more irregular, less energetically favorable configurations being frozen into the crystal.

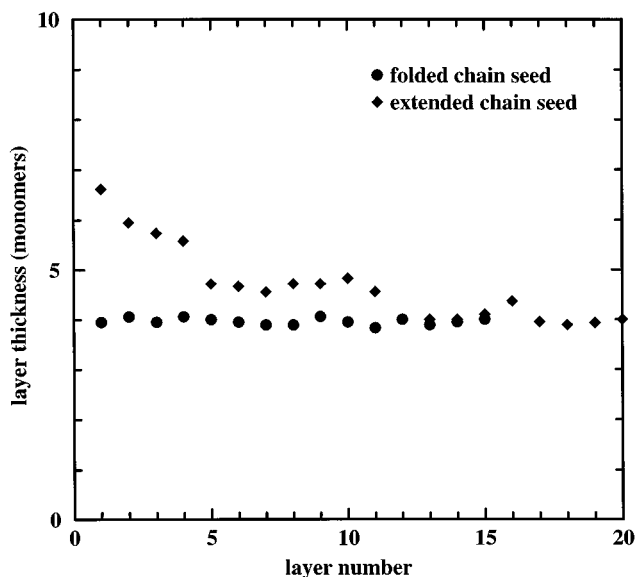


FIG. 9. Layer thickness of folded chain crystals growing from a seed of folded chains and a seed of extended chains. The thickness of both crystals is about 4 monomers.

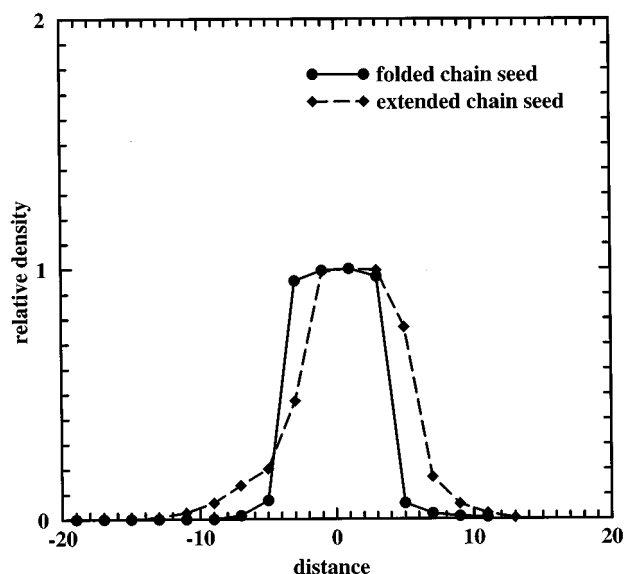


FIG. 10. Density profile of folded chain crystals as a function of distance away from the center of the seed. For the crystal with a seed of folded chains, the density profile has sharp boundaries. For the crystal with a seed of extended chains, the density profile is due to a mismatch of two half-folded chain crystals.

## V. CRYSTALLIZATION OF EXTREMELY LONG POLYMER CHAINS IN DILUTE SOLUTION

In the crystallization of monodisperse polymer chains, the chain length is a characteristic length scale which determines the crystal thickness, i.e., a marked preference for integer folding is observed. For infinitely long polymer chains or polydisperse polymer chains, there is no characteristic length scale of the system and we expect a continuous change of crystal thickness when the temperature varies. In this section, we study the crystallization of long polymer chains in dilute solution in which case the chain length of polymers is much greater than the crystal thickness. The simulations were done by depositing a polymer chain on a seed and allowing it to crystallize due to attraction between bonds. In a very dilute solution, there is only one chain attached on the surface of a crystal at a time. In the simulation, a long polymer chain is treated in such way that it consists of a crystallized, folded chain part plus a dangling end of a few effective monomers. An additional monomer is added to (or removed from) the dangling end whenever a monomer is crystallized (or dissolved), such that the number of monomers in the dangling end is constant. Another chain can land on the surface of the crystal only when the previous chain has crystallized. This would correspond to a terrace growth of the crystal. This simulation results in a crystal with one long chain in each layer. These simplifications have been introduced into the program in order to speed it up. Dealing with simultaneous motion of many long chains would be too slow to simulate with our currently available computers.

Figure 13 shows the resulting crystal from simulation at  $T=0.55$  and  $e=1.0$ , and the thickness of the seed is  $l_{\text{seed}}=6$  monomers. The average thickness of this crystal is 5.6 monomers. The crystal surfaces are rough and there are many

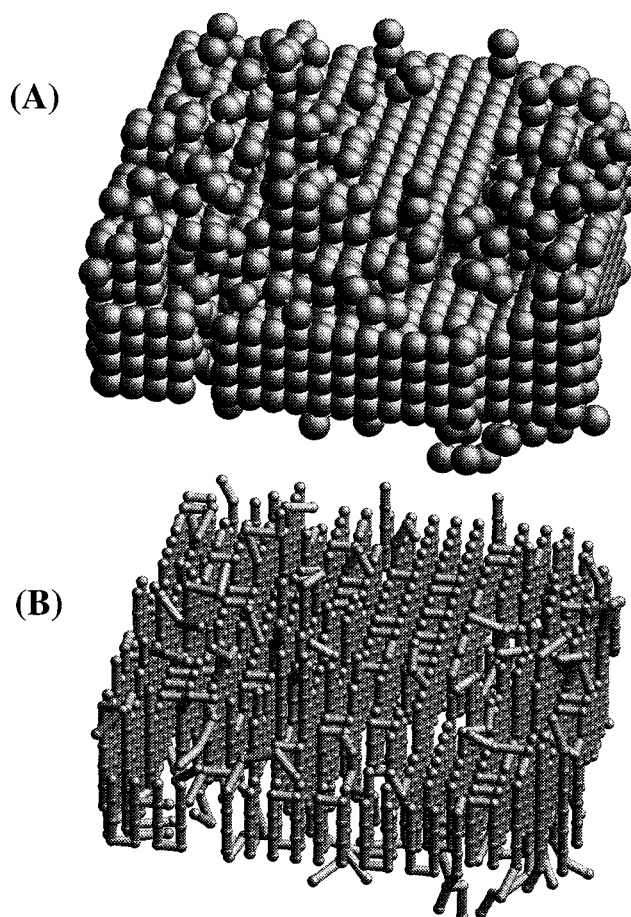


FIG. 11. Schematic representations of surfaces (A) and bond configuration (B) of a folded chain crystal obtained from the Monte-Carlo simulation with a seed of folded chains at  $T=0.4$ . The stiffness parameter of polymer chains is  $e=0.8$ . Both extended chains and folded chains present in this crystal. The crystal also contains a few holes.

loops on the surfaces. Large loops are possible if we use a long dangling end. Figure 14 shows the layer thickness of crystals growing from three different seeds of thickness 5, 6, and 7 monomers respectively. As demonstrated in the Sadler/Gilmer model,<sup>9-11</sup> the average layer thickness is determined by the competition between an energetic driving term and an entropic barrier term. For  $l_{\text{seed}}=5$  monomers, the layer thickness of the crystal increases as the crystal grows due to the energetic driving term. For  $l_{\text{seed}}\geq 6$  monomers, the layer thickness of the crystals decreases as the crystals grow due to the entropic barrier term. The dependence of the average crystal thickness on temperature is shown in Fig. 15. The average thickness increases with temperature  $T$  and diverges at  $T=T_{\infty}\approx 0.675$ . The theoretical minimum stable thickness ( $l_{\text{min}}$ ) for the crystal is calculated in the Appendix. The difference between the average thickness and  $l_{\text{min}}$  decreases as  $T$  approaches  $T_{\infty}$ . This is because the barrier term becomes more important at high temperatures, while the driving term becomes more important at low temperatures. Therefore, for  $T$  close to  $T_{\infty}$ , the average thickness of the crystal is approximately  $l_{\text{min}}$ .

Since the length of the dangling end is kept fixed and is relatively short, there is no possibility of forming large loops at the fold surface which in principle could occur. We ex-

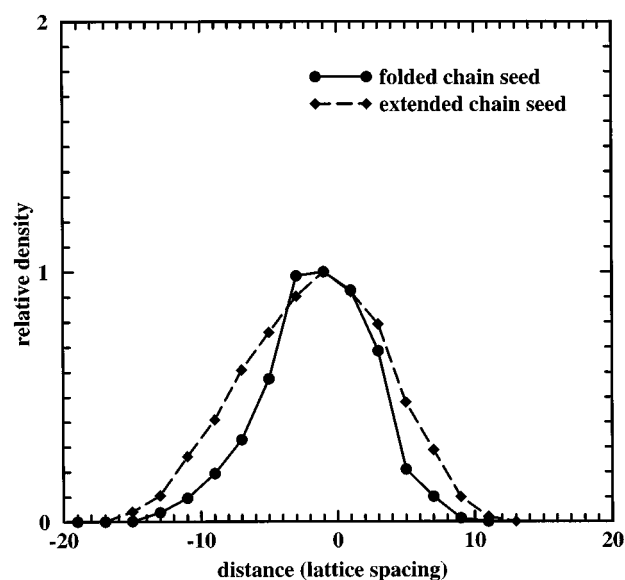


FIG. 12. Density profile of folded chain crystals as a function of distance away from the center of the seed. Simulations were performed at  $T=0.4$  and  $e=0.8$ . For the crystal with a seed of folded chains, the density profile is due to a mismatch of two half-folded chain crystals bridged by extended chains. For the crystal with a seed of extended chains, the density profile shows a broad peak. Both density profiles are much broader and the boundaries are much less sharp than those in Fig. 10.

perimented with varying the length of the dangling end and found that increasing the length led to very much slower simulations but did not change the chain configurations at the fold surface, i.e., large loops almost never occurred in the simulations. It was also found that occasionally very short stems became incorporated into one crystal layer. These behave as defects which strongly slow down the rate of growth

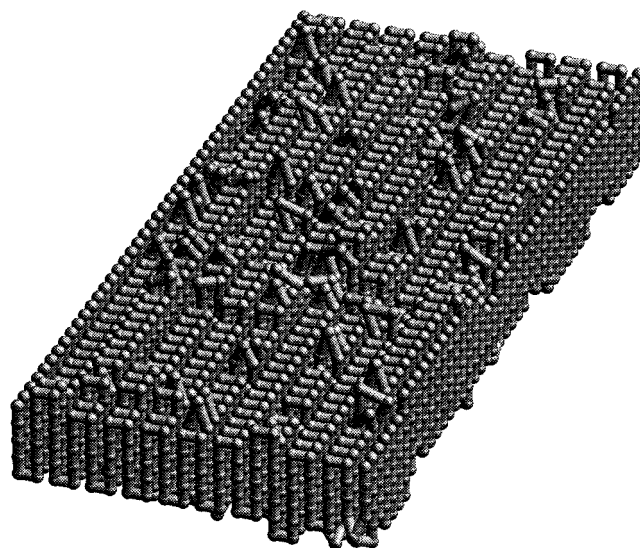


FIG. 13. Schematic representation of bond configurations of a crystal obtained from the Monte-Carlo simulation of crystallization of long polymer chains (one chain per layer). The stiffness parameter of polymer chains is  $e=1$ . The crystal has a rough surface with many loops.

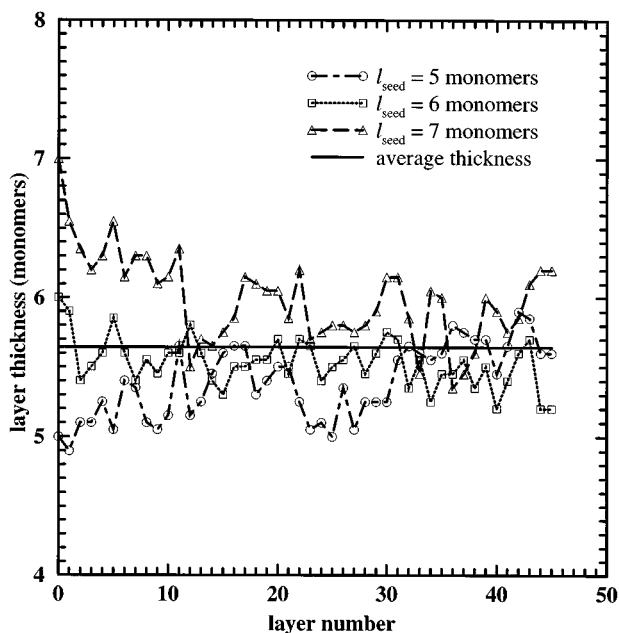


FIG. 14. Layer thickness of crystals crystallized from long chains with a seed of thickness  $l_{\text{seed}} = 5, 6,$  and  $7$  monomers. Simulations were done at  $T=0.55$  and  $e=1$ . The average thickness is  $5.64$  monomers. If the initial seed thickness is slightly below or above this value, the thickness gradually adjusts to the preferred value.

of the next layer past this point. In a real crystal we would expect some degree of chain sliding and evening out of monomers between adjacent stems. The probability for sliding a stem within the crystal in this simulation is extremely small, so that short stem defects can never heal themselves. In order to prevent the simulation getting stuck at such defects for extremely long times we introduced the following

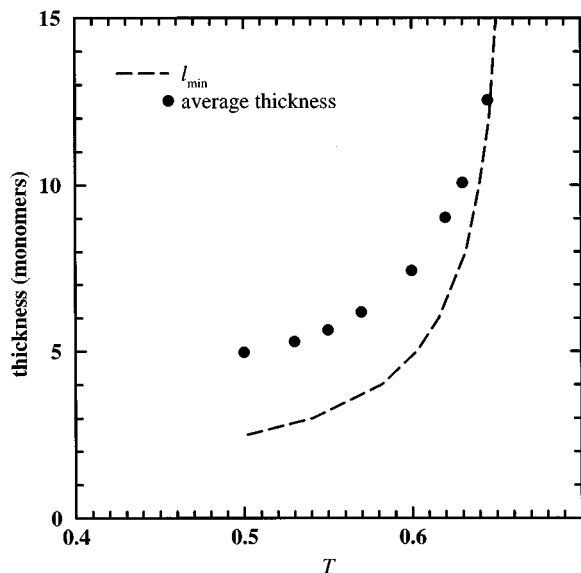


FIG. 15. The average thickness of crystals crystallized from extremely long chains as a function of temperature  $T$ . The data are results from Monte-Carlo simulation of crystallization of extremely long chains. The dashed line is a theoretic curve of the minimum growth thickness of the crystal.

rule for removal of defects. If the growth surface of the crystal contained stems which were much smaller than  $l_{\text{min}}$ , and which remained so for a long time, we increased their length to the average stem length of the layer. We note that the growth rate of the crystal will be greatly affected by this simplification, and therefore a more realistic mechanism for thickening those short stems would be required if we wished to measure the growth rate. However we checked that this procedure did not have much effect on the crystal thickness. For this reason only results on crystal thickness and not on growth rate are given here for long chains.

## VI. DISCUSSION AND CONCLUSIONS

In this paper, we have used the three-dimensional bond fluctuation model to study the crystallization of monodisperse polymers and extremely long polymers in dilute solution. We believe that these are the first simulations of crystallization which take into account realistic motions of chain segments and which deal with the simultaneous motions of many chains. Previous simulations such as those of Sadler and Gilmer<sup>9</sup> and our own previous work<sup>17</sup> only considered lattice sites in the crystal as occupied or empty. They did not properly account for the kinetics of the chains as they adsorb to the crystal. Alternative approaches using molecular dynamics<sup>23</sup> deal with atomic scale motions realistically but cannot cope with large scale phenomena involving many chains. The level of resolution given by the bond fluctuation model is therefore very useful for this problem. Each bond vector of the model represents a length of the real chain approximately equal to its persistence length. Such a coarse-grained model can greatly improve the speed of simulations without losing important information.

The dominant driving force of the crystallization comes from the short range attraction between polymer segments. We model this attractive force by an interaction between parallel bonds, rather than between neighboring effective monomers. This type of interaction is important for polymer crystallization since the bond-bond interaction breaks the isotropic symmetry and leads to the formation of a lamellar crystal. On the other hand, the monomer-monomer interaction does not break the isotropic symmetry and hence a three-dimensional crystal is preferred. We experimented with a range of models including only monomer-monomer interaction and combinations of monomer-monomer and bond-bond interactions. All these tended to lead to irregular three dimensional aggregates with no preferred chain orientation. For simulations with interactions including both monomer-monomer and bond-bond attraction, we always see three-dimensional crystals consisting of domains of two-dimensional crystals in three directions as the crystals grow. Bond-bond interaction alone was therefore used for the results presented here. It has been shown that lamellar crystals are observed in various experiments, which shows the importance of chain connectivity. Our model has properly considered both the entropic barrier and chain connectivity during polymer crystallization.

Our model also confirms the previous idea of the self-poisoning effect on the crystallization of monodisperse polymers. Both extended chain crystals and once-folded chain

crystals are seen in our simulations. The temperature ranges for both crystals to grow are estimated in the Appendix, and are found to be consistent with the simulation results. Furthermore, our simulations show that the folding kinetics of polymer chains during crystallization is also related to the stiffness parameter (or kink energy) of polymers, in addition to the global flexibility of polymer chains. In our simulations, we have shown that polymer chains with small stiffness parameter can lead to a once-folded chain crystal with a sharp boundary and few defects at temperature below  $T_2$ . However, polymer chains with a large stiffness parameter form irregular crystals with both folded and extended chains. Since the extended chains in the crystal can bridge two folded chain crystals, mismatch can happen easily for such crystals.

Long polymer chains can fold many times in the crystal. The crystal thickness diverges as  $T \rightarrow T_\infty$ . At low temperatures, the energetic driving term is more important than the entropic barrier term, and the average crystal thickness is larger than the minimum crystal thickness  $l_{\min}$ . At high temperatures, the entropic barrier term becomes dominantly important and the average thickness is close to  $l_{\min}$ .

In conclusion, we have demonstrated the importance of folding kinetics on polymer crystallization by three-dimensional Monte-Carlo simulations using the bond fluctuation model. Both entropic barrier and chain connectivity play an important role during crystallization. We have also shown that large stiffness of polymer chains increases the amount of defects in folded chain crystals. The characteristic properties of monodisperse chains have been shown to lead to an ‘integer folding’ of polymer crystallization, which is absent for extremely long chains or polydisperse chains.

## ACKNOWLEDGMENTS

We are grateful to Dr. G. Ungar for his useful suggestions and comments on our work. The authors acknowledge the support from EPSRC under Grant No. GR/K/67922.

## APPENDIX: CALCULATION OF CRYSTALLIZATION TEMPERATURES

The crystallization temperatures  $T_1$  and  $T_2$  can be estimated as follows. The free energy per chain in a solution can be approximated by

$$F_{\text{sol}} = -T \ln \Gamma_N + T \ln \phi, \quad (\text{A1})$$

where  $\Gamma_N$  is the number of configurations of a self-avoiding walk of  $N$  steps ( $N = n_m - 1$ , where  $n_m$  is the number of monomers per chain), and  $\phi$  is the concentration of chains. From the theory of self-avoiding walks,<sup>24</sup> we expect that

$$\Gamma_N \approx cN^{\gamma-1} \tilde{z}^N, \quad (\text{A2})$$

where  $\gamma \approx 7/6$  in three dimensions, and  $\tilde{z}$  should be somewhat less than 108 due to excluded volume constraints. We obtained  $\Gamma_N$  by exact enumeration for  $N \leq 6$ , and found that Eq. (A2) fits the data almost perfectly when  $c = 1.26$  and  $\tilde{z} = 85.2$ , as shown in Fig. 16. The second term in Eq. (A1) is the translational entropy of the chains in the ideal gas approximation, which is reasonable for a dilute solution. We

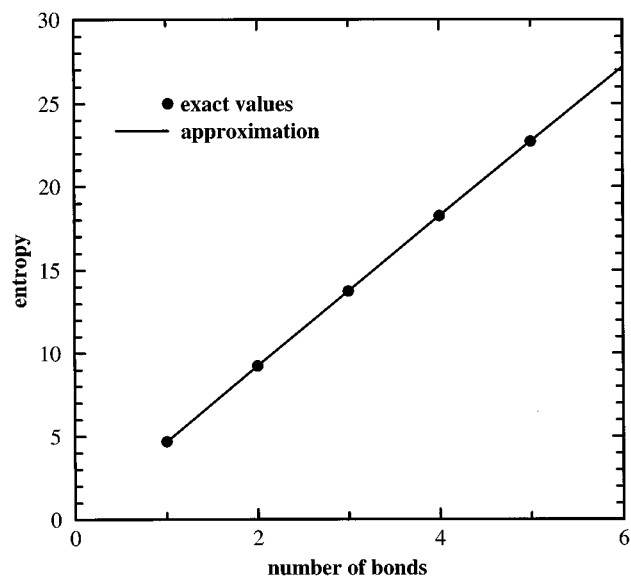


FIG. 16. The entropy of polymer bond configurations (i.e.,  $\ln \Gamma_N$ ) as a function of number of bonds. The data points from exact numerical calculation fit almost perfectly with the approximation in Eq. (A2).

have neglected energetic terms in the free energy of polymer chains in solution since these terms have negligible effect over the range of temperatures of interest here (as was shown in Fig. 2).

The free energy of a perfect crystal is entirely energetic. For a perfect extended chain crystal with chains of  $n_m$  monomers, the free energy per chain is

$$F_{\text{ext}} = -2n_m + 2 - e(n_m - 2). \quad (\text{A3})$$

For a perfect once-folded chain crystal with even  $n_m$ , the free energy per chain is

$$F_{\text{fold}} = -2n_m + h_f - e(n_m - 4), \quad (\text{A4})$$

where  $h_f = 3$  if all polymer chains fold on the same surface or  $h_f = 4$  if attraction between folded bonds is neglected. For resulting folded chain crystals from the simulations, the number of folds of the chains on top and bottom surfaces is almost the same, and we expect  $3 \leq h_f \leq 4$ .

To calculate  $T_1$  and  $T_2$ , we compare the free energy of polymer chains in solution ( $F_{\text{sol}}$ ) and in crystals ( $F_{\text{ext}}$  or  $F_{\text{fold}}$ ). The crystallization temperature  $T_1$  for an extended chain crystal can then be expressed by

$$T_1 \approx \frac{2n_m - 2 + (n_m - 2)e}{\ln c + \frac{1}{6} \ln(n_m - 1) + (n_m - 1) \ln \tilde{z} - \ln \phi}. \quad (\text{A5})$$

Similarly, the temperature for a once-folded chain crystal is

$$T_2 \approx \frac{2n_m - h_f + (n_m - 4)e}{\ln c + \frac{1}{6} \ln(n_m - 1) + (n_m - 1) \ln \tilde{z} - \ln \phi}. \quad (\text{A6})$$

For  $n_m = 8$ ,  $e = 0.6$ ,  $\phi \approx 0.006$ , and  $h_f = 3.5$ , we have  $T_1 \approx 0.48$  and  $T_2 \approx 0.41$ .

For long polymer chains, the relationship between minimum crystal thickness  $l_{\min}$  and  $T$  can be expressed as

$$T \approx \frac{2l_{\min} + (l_{\min} - 1)e}{\ln c + \frac{1}{6} \ln l_{\min} + l_{\min} \ln \tilde{z}} \quad (\text{A7})$$

by comparing the free energy of polymer chains in solution and in crystal. Here, the concentration of polymer chains does not enter Eq. (A7) since polymer chains are fixed on the crystal surface when they are placed.

- <sup>1</sup>K. Armistead and G. Goldbeck-Wood *Adv. Polym. Sci.* **100**, 219 (1992).  
<sup>2</sup>J. I. Lauritzen and J. D. Hoffman, *J. Res. Bur. Stand.* **64A**, 73 (1960); J. D. Hoffman and J. I. Lauritzen *ibid.* **65A**, 297 (1961); J. D. Hoffman, C. M. Guttman, and E. A. DiMarzio, *Discuss. Faraday Soc.* **68**, 177 (1979).  
<sup>3</sup>J. D. Hoffman, *Polymer* **32**, 2828 (1991); **33**, 2643 (1992).  
<sup>4</sup>A. Toda, *J. Phys. Soc. Jpn.* **55**, 3419 (1986); *Faraday Discuss.* **95**, 129 (1993).  
<sup>5</sup>M. L. Mansfield, *Polymer* **29**, 1755 (1988).  
<sup>6</sup>J. J. Point and D. Villers, *Polymer* **33**, 2263 (1992).  
<sup>7</sup>D. Wunderlich and A. Mehta, *J. Polym. Sci., Polym. Phys. Ed.* **12**, 255 (1974).  
<sup>8</sup>M. Hikosaka, *Polymer* **28**, 1257 (1987); **31**, 458 (1990).  
<sup>9</sup>D. M. Sadler and G. H. Gilmer, *Polymer* **25**, 1446 (1984); *Phys. Rev. Lett.* **56**, 2708 (1986).  
<sup>10</sup>D. M. Sadler, *Nature (London)* **326**, 174 (1987).  
<sup>11</sup>M. A. Spinner, R. W. Watkins, and G. Goldbeck-Wood, *J. Chem. Soc. Faraday Trans.* **91**, 2587 (1995); G. Goldbeck-Wood, *Macromol. Symp.* **81**, 221 (1994); *Polymer* **33**, 779 (1992).

- <sup>12</sup>I. Bidd and M. C. Whiting, *J. Chem. Soc. Chem. Commun.* **1985**, 543; I. Bidd, D. W. Holdup, and M. C. Whiting, *J. Chem. Soc. Perkin Trans.* **1**, 2455 (1987).  
<sup>13</sup>G. Ungar and A. Keller, *Polymer* **28**, 1899 (1987).  
<sup>14</sup>S. J. Organ, G. Ungar, and A. Keller, *Macromolecules* **22**, 1995 (1989); S. J. Organ, A. Keller, M. Hikosaka, and G. Ungar, *Polymer* **37**, 2517 (1996).  
<sup>15</sup>G. Ungar, J. Stejny, A. Keller, and M. C. Whiting, *Science* **229**, 386 (1985).  
<sup>16</sup>D. M. Sadler and G. H. Gilmer, *Polym. Commun.* **28**, 242 (1987).  
<sup>17</sup>P. G. Higgs and G. Ungar, *J. Chem. Phys.* **100**, 640 (1994).  
<sup>18</sup>I. Carmesin and K. Kremer, *Macromolecules* **21**, 2819 (1988).  
<sup>19</sup>W. Paul, K. Binder, D. W. Heermann, and K. Kremer, *J. Chem. Phys.* **95**, 7726 (1991); I. Gerroff, A. Milchev, K. Binder, and W. Paul, *J. Chem. Phys.* **98**, 6526 (1993).  
<sup>20</sup>H. P. Deutsch and K. Binder, *J. Chem. Phys.* **94**, 2294 (1991).  
<sup>21</sup>H.-P. Wittmann, K. Kremer, and K. Binder, *J. Chem. Phys.* **96**, 6291 (1992); P. Ray, J. Baschnagel, and K. Binder, *J. Phys.: Condens. Matter* **5**, 5731 (1993).  
<sup>22</sup>M. Müller, K. Binder, and W. Oed, *J. Chem. Soc. Faraday Trans.* **91**, 2369 (1995); M. Müller and M. Schick, *J. Chem. Phys.* **105**, 8885 (1996).  
<sup>23</sup>P. R. Sundararajan and T. A. Kavassalis, *J. Chem. Soc. Faraday Trans.* **91**, 2541 (1995).  
<sup>24</sup>P. G. de Gennes, *Scaling Concepts in Polymer Physics* (Cornell University Press, Ithaca, 1988).